Letter

Effects of discrete topology on quantum transport across a graphene *n-p-n* junction: A quantum gravity analog

Naveed Ahmad Shah,[1,*] Alonso Contreras-Astorga,[2,†] François Fillion-Gourdeau,[3,4,‡] M. A. H. Ahsan,[1,§] Steve MacLean,[3,4,5,‖] and Mir Faizal[6,7,8,¶]

[1]*Department of Physics, Jamia Millia Islamia, New Delhi 110025, India*
[2]*CONACyT-Physics Department, Cinvestav, P.O. Box. 14-740, 07000 Mexico City, Mexico*
[3]*Institute for Quantum Computing, University of Waterloo, Waterloo, Ontario, Canada N2L 3G1*
[4]*Infinite Potential Laboratories, Waterloo, Ontario, Canada N2L 0A9*
[5]*Université du Québec, INRS-Énergie, Matériaux et Télécommunications, Varennes, Québec, Canada J3X 1S2*
[6]*Irving K. Barber School of Arts and Sciences, University of British Columbia - Okanagan, Kelowna, British Columbia, Canada V1V 1V7*
[7]*Department of Physics and Astronomy, University of Lethbridge, Lethbridge, Alberta, Canada T1K 3M4*
[8]*Canadian Quantum Research Center, 3002 32nd Avenue, 204, Vernon, British Columbia, Canada V1T 2L7*

(Received 16 December 2021; revised 21 March 2022; accepted 23 March 2022; published 6 April 2022)

In this Letter, we investigate the effect of next-to-nearest atom hopping on Klein tunneling in graphene. An effective quantum dynamics equation is obtained based on an emergent generalized Dirac structure by analyzing the tight-binding model beyond the linear regime. We show that this structure has some interesting theoretical properties. First, it can be used to simplify quantum transport calculations used to characterize Klein tunneling; second, it is not chirally symmetric as hinted by previous work. Finally, it is reminiscent of theories on a space with a discrete topology. Exploiting these properties, we show that the discrete topology of the crystal lattice has an effect on the Klein tunneling, which can be experimentally probed by measuring the transmittance through *n-p-n* junctions. We argue that this simulates some quantum gravity models using graphene and we propose an experiment to perform such measurements.

DOI: 10.1103/PhysRevB.105.L161401

At low energies, the quasiparticles of graphene responsible for its transport properties have a well-known description in terms of an emergent Dirac field theory [1–3]. This property stems from the symmetries of the underlying honeycomb two-dimensional (2D) lattice, which reduces to a Dirac-like structure in the low-energy limit. The fact that the Dirac equation describes charge carriers makes graphene a testbed for relativistic theories in a nonrelativistic setting and it allows for the simulation of quantum electrodynamics (QED) in a condensed matter system [4–11].

Klein tunneling was one of the first QED-like effects to be investigated in graphene [12,13]. This relativisticlike phenomenon corresponds to the unimpeded transmission of particles through a potential step. Owing to the presence of negative energy states, there is no exponential damping and particles are almost fully transmitted when the potential barrier is larger than the rest mass energy of the particles. In graphene, conductance in transport experiments through *p-n* junctions is the main observable used to detect this effect experimentally because Klein tunneling has a strong effect on the transmittance [14–18]. The results of these experiments using electrostatic barriers were theoretically understood using the Dirac theory with the presence of negative energy states below the potential [19–21]. Although much work has been done in monolayer graphene [22–27] and other condensed matter systems [28], the theoretical analysis were, for the most part, limited to the linear approximation (low-energy limit) in the tight-binding model, where a standard Dirac structure exists.

Some research on quantum transport has gone beyond this linear regime by studying various limits of the tight-binding model. In principle, these approaches are more accurate for the calculation of transport properties, especially at higher energies. For instance, implications of the next-to-nearest hopping term on doping and Klein tunneling have been investigated in Ref. [29]. Within this approximation, it has been observed that the tunneling is no longer chiral and that an asymmetry occurs on conductance curves around the perfect transmission point. Furthermore, the effects of the trigonal warping terms [30–33] and deformed lattices [34] on transmittance have been considered. In particular, the Klein tunneling beyond the linear approximation has been studied using a generalized pseudospin mode-matching technique in the tight-binding model [30]. This last approach shares many similarities with the technique presented in this paper.

In this Letter, we investigate Klein tunneling beyond the linear approximation in monolayer graphene by including the next-to-nearest atom hopping. This is performed by

*naveed179755@st.jmi.ac.in
†alonso.contreras@conacyt.mx
‡francois.fillion@inrs.ca
§mahsan@jmi.ac.in
‖steve.maclean@inrs.ca
¶mirfaizalmir@googlemail.com

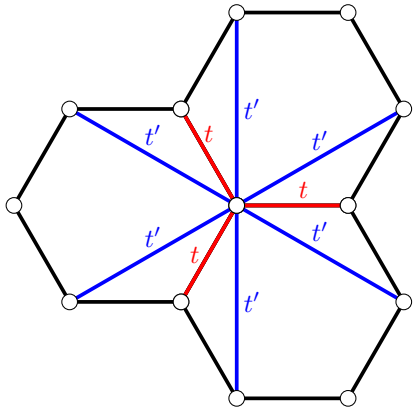

FIG. 1. Graphene hexagonal lattice with nearest (t) and next-to-nearest (t') hopping energies.

introducing a generalized Dirac structure (GDS), which allows for straightforward mode-matching calculations of the transmittance in the continuum limit. We argue that graphene beyond the linear regime can be used as a quantum gravity analog. Indeed, the Dirac structure emerging in this limit is precisely of the kind obtained in quantum gravity models with a minimal length scenario [35–39]. Based on this physical insight, we show that Klein tunneling at intermediate energy is sensitive to the minimal length set by the lattice constant and, thus, actually probes the underlying space topology. This effect simulates the effect of quantum gravity models on particle transport. Finally, we evaluate the transmittance in an n-p-n junction and we make a proposal to measure these effects experimentally.

The effects of discrete topology of graphene can be investigated using its tight-binding model. In a tight-binding model of graphene, the electron dispersion relation, expanded to $O((ka)^2)$, is given by [3,29,40,41]

$$\epsilon_{\boldsymbol{k}}^{\lambda} = \lambda\hbar v_F k + \frac{9a^2}{4}t'k^2 - \lambda\frac{\hbar v_F k^2 a}{4}\cos(3\phi_{\boldsymbol{k}}), \tag{1}$$

where $\lambda = \pm 1$ is the band index, $v_F = 3ta/2\hbar$ is the Fermi velocity, $k = |\boldsymbol{k}|$ is the wave-vector magnitude, and t and t' are the nearest- and the next-to-nearest-neighbor hopping energies (see Fig. 1) while $a = 1.4$ Å is the lattice constant. Also, $\phi_{\boldsymbol{k}} = \arctan(k_y/k_x)$ is the azimuthal angle of the wave vector with respect to the x axis. The dispersion relation [Eq. (1)] comprises three different terms: the first term is the low-energy linear contribution, the second one appears as the low-energy limit of the next-to-nearest-neighbor hopping, and the third term, called trigonal warping, is the next-to-leading-order contribution obtained from the low-energy limit of the tight-binding model with nearest-neighbor hopping. We can see from the above equation that the t' correction breaks the electron-hole (chiral) symmetry in the sense that $\epsilon_{\boldsymbol{k}}^{-\lambda} \neq -\epsilon_{\boldsymbol{k}}^{\lambda}$.

The dispersion relation for massless particles in many quantum gravity models is rotationally symmetric, of the form $\epsilon_{\text{grav},\boldsymbol{p}} = F(p)$, where F is usually a polynomial function and $\boldsymbol{p} = \hbar\boldsymbol{k}$ is now the momentum, related to the wave vector via de Broglie relations. One particular model has been extensively studied in which the dispersion relation is given by $\epsilon_{\text{grav},\boldsymbol{p}} = c_1 p + c_2 p^2$, where $c_{1,2}$ are some coefficients [42–44]. This dispersion relation explicitly breaks Lorentz invariance even though it is rotationally invariant because it is not conserving the four-momentum of a particle.

We make a connection between graphene and quantum gravity models by neglecting the trigonal warping term. Because this term encodes the symmetry of the lattice and breaks rotational invariance, it can be neglected for small angular regions around the angles $\phi_{\boldsymbol{k}}^{\delta} = (2n+1)\frac{\pi}{6} \pm \delta$ with $n \in \mathbb{N}$ and where $\delta = \frac{1}{3}\sin^{-1}(\frac{3|t'|}{5t}) \approx 0.02$. In this angular region, we have $\cos(3\phi_{\boldsymbol{k}}) \approx 0$. Assuming all processes occur in a momentum region where we can neglect the trigonal warping term and renaming some variables, the energy becomes

$$\epsilon_{\boldsymbol{p}}^{\lambda} = v_F(\lambda p - \alpha p^2), \tag{2}$$

where $\alpha = \frac{3}{2}\frac{|t'|}{t}\frac{a}{\hbar} > 0$. Obviously, this has the same form as $\epsilon_{\text{grav},\boldsymbol{p}}$ with the connection provided by the mapping $c_1 \to v_F\lambda$ and $c_2 \to -v_F\alpha$.

To derive a dynamical Dirac-like equation having a dispersion relation given by Eq. (2), we borrow the technique developed for quantum gravity models with minimal lengths. As demonstrated in Ref. [45], this can be performed by following the Dirac prescription $p \to \boldsymbol{\sigma}\cdot\hat{\boldsymbol{p}}$ in the expression for the energy, where $\hat{\boldsymbol{p}} = -i\hbar\boldsymbol{\nabla}$ is now the momentum operator and $\boldsymbol{\sigma}$ are Pauli matrices. We use the Dirac prescription and represent SO(2)-invariant vectors in their spinor representation. This yields the Hamiltonian operator given by

$$\begin{aligned}\hat{H} &= v_F[\boldsymbol{\sigma}\cdot\hat{\boldsymbol{p}} - \alpha(\boldsymbol{\sigma}\cdot\hat{\boldsymbol{p}})(\boldsymbol{\sigma}\cdot\hat{\boldsymbol{p}})] \\ &= v_F[\boldsymbol{\sigma}\cdot\hat{\boldsymbol{p}} - \alpha\hat{p}^2\sigma_0],\end{aligned} \tag{3}$$

where $\sigma_0 = \mathbb{I}_2$ is the unit matrix. This procedure reproduces the low-energy limit of the next-to-nearest-neighbor Hamiltonian contribution at next-to-leading order [40]. To emphasize the fact that $\hat{H}$ has a GDS, the corresponding dynamical equation is now given:

$$i\hbar\partial_t\psi(t,\boldsymbol{x}) = v_F(\boldsymbol{\sigma}\cdot\tilde{\boldsymbol{P}})\psi(t,\boldsymbol{x}), \tag{4}$$

where $\tilde{\boldsymbol{P}} = \hat{\boldsymbol{p}}\sigma_0 - \boldsymbol{\sigma}\alpha\hat{p}^2$ and where ψ is the two-component spinor wave function. Equation (4) is a generalized massless Dirac equation. In addition, it can be readily tested that the dispersion relation obtained from the energy eigenvalue equation for the above (see Eq. (12) in Ref. [46]) is the same as Eq. (2).

The mathematical structure defined thus far by the GDS in Eq. (4) and the dispersion relation in Eq. (2) is consistent with the framework of the generalized uncertainty principle (GUP). In this framework, one postulates the existence of generalized position and momentum operators, $\hat{\boldsymbol{X}}$ and $\hat{\boldsymbol{P}}$, that obey a modified commutation relation (see Sec. A in Ref. [46]):

$$[\hat{X}_i, \hat{P}_j] = i\hbar\left[\delta_{ij} - \alpha\left(\delta_{ij}\hat{P} + \frac{\hat{P}_i\hat{P}_j}{\hat{P}}\right)\right]. \tag{5}$$

These relations imply a minimal measurable length $(\Delta x)_{\min} \sim \hbar\alpha$ and a maximal measurable momentum $(\Delta p)_{\min} \sim \alpha^{-1}$ [45,47]. Therefore, in this formalism, $\alpha \propto a$ is a parameter that captures the effect of the discrete topology. It appears in our description of graphene owing to the discreteness of its atomic structure. A similar technique, based on a deformation of the Heisenberg algebra, has been considered for the calcu-

lation of the optical conductivity with next-to-leading-order corrections at zero and finite temperature [48–50].

To obey the generalized commutation relations (5), the generalized position and momentum operators must be related to the usual position and momentum operators as $\hat{\boldsymbol{X}} = \hat{\boldsymbol{x}}$ and $\hat{\boldsymbol{P}} = \hat{\boldsymbol{p}}(1 - \alpha\hat{p})$, with $[\hat{x}_i, \hat{p}_j] = i\hbar\delta_{ij}$. The operators $\hat{\boldsymbol{X}}$ and $\hat{\boldsymbol{P}}$ can be interpreted as the high-energy position and momentum, respectively, while $\hat{\boldsymbol{x}}$ and $\hat{\boldsymbol{p}}$ are their low-energy counterparts [35]. The definition of the generalized momentum can be understood as a rotational-symmetric energy-scale transformation. The Dirac-like equation obtained from this formalism has the form given in Eq. (4) when one replaces the momentum operator by the generalized one and by using the Dirac prescription [35,45].

As expected from the dispersion relation, the full Lorentz symmetry is not preserved in this mathematical structure and this implies particle-hole asymmetry. This symmetry breaking is algebraically indicated by the presence of $\hat{P}_i\hat{P}_j/\hat{P}$ terms in the commutation relations (5). Thus, chiral symmetry breaking arises from a more fundamental, although a less stringent, phenomenon of Lorentz symmetry breaking, which is reminiscent of the discrete topology of the space itself. It is less stringent, because we still consider the space to be isotropic (which shows up as the SO(2) symmetry).

It is interesting to note that the algebraic structure induced by the GUP also occurs in some quantum gravity models [35,36,38,39], where the Planck length plays a role analogous to interatomic length in graphene. Actually, this formalism was developed to be consistent with string theory, black hole physics, and doubly special relativity [45,47]. In gravitational theories, however, we have $\alpha \sim \ell_{\text{plank}}/\hbar$, where ℓ_{plank} is the Planck length. As a consequence, nonlinear corrections to the dispersion are very weak, unless one probes the system at Planck energy scales. This is not possible with actual experimental apparatus.

On the other hand, nonlinear corrections in graphene start to be important at much lower energy scales [41]. Furthermore, as demonstrated in this article, it follows an algebraic structure consistent with GUP for some specific angles $\phi_{\boldsymbol{k}}$. Therefore, it is interesting to look at phenomenological implications of these corrections as they can be used as quantum gravity analogs. For this purpose, we analyze Klein tunneling at intermediate energies (∼100 meV) to investigate the effects of the α term on this phenomenon.

To study Klein tunneling, we consider free waves scattering on an *n-p-n* junction (more details of this calculation can be found in Sec. B of Ref. [46]). Thus, an electric static barrier potential $V(x) = V_0\Theta(x)\Theta(D - x)$, where D is the potential length, is introduced in the GDS, resulting in

$$\begin{aligned}\hat{H}\ \Psi(\boldsymbol{r}) &= \{v_F[-i\hbar\boldsymbol{\sigma}\cdot\boldsymbol{\nabla} + \alpha\hbar^2\,\sigma_0\,\nabla^2] + V(x)\}\Psi(\boldsymbol{r}) \\ &= E_G\ \Psi(\boldsymbol{r}).\end{aligned} \tag{6}$$

Here (as in ordinary Klein tunneling [19,20]) the potential barrier distinguishes three different regions: region A [$V(x) = 0$, $x \leqslant 0$], with an incoming wave and a reflected one from the interface at $x = 0$; region B [$V(x) = V_0$, $0 < x \leqslant D$], with two waves, one transmitted from region A and another reflected by the interface at $x = D$; and region C [$V(x) = 0, x > D$], where there is just a transmitted wave. In the piecewise constant potential $V(x)$, Eq. (6) admits plane-wave solutions $\Psi(\boldsymbol{x}) = e^{ik_y y}\varphi(x)$, where

$$\varphi(x) = \begin{cases} e^{ik_x x}\begin{pmatrix}1\\ e^{i\phi}\end{pmatrix} + \mathcal{R}e^{-ik_x x}\begin{pmatrix}1\\ -e^{-i\phi}\end{pmatrix}, & x < 0; \\ ae^{iq_x x}\begin{pmatrix}1\\ -e^{i\theta}\end{pmatrix} + be^{-iq_x x}\begin{pmatrix}1\\ e^{-i\theta}\end{pmatrix}, & 0 < x \leqslant D; \\ \mathcal{T}e^{ik_x x}\begin{pmatrix}1\\ e^{i\phi}\end{pmatrix}, & x > D; \end{cases} \tag{7}$$

In the above, $\mathcal{R}$ and $\mathcal{T}$ are the reflection and transmission coefficients, respectively, while a and b are the coefficients of the waves under the barrier. Also, $\boldsymbol{k}$ is the wave vector in regions A and C while $\boldsymbol{q}$ is the wave vector in region B. The angles $\phi = \arctan(k_y/k_x)$ and $\theta = \arctan(q_y/q_x)$ are the incident and transmitted angles, respectively. Since the potential $V(x)$ is translationally invariant along the y axis, the projection of the wave vector k_y is a conserved quantity and we have $k_y = q_y$. Without loss of generality, we will assume $k_y > 0$, representing an electron traveling from the lower half plane $y < 0$ to the upper half plane $y > 0$. Moreover, we will restrict ourselves to the energy range $0 < E_G < V_0$, where the Klein tunneling phenomenon occurs. The energy E_G in region A is related to k via Eq. (2). Also, we can find q_x in region B:

$$\begin{aligned}q_x^2 = \frac{1}{(2\alpha\hbar)^2}\Bigg(2 - \frac{4\alpha(E_G - V_0)}{v_F} \\ - 2\sqrt{1 - \frac{4\alpha(E_G - V_0)}{v_F}}\Bigg) - k^2\sin^2\phi.\end{aligned} \tag{8}$$

The transmitted angle θ can be found using $\tan\theta = (k\sin\phi/q_x)$. Then matching the modes, i.e., equating the spinors in the three regions at the two boundaries of the potential assuming the continuity of the solution $\Psi(x, y)$ at $x = 0$ and $x = D$, gives us the conditions on the coefficients of the spinors. Solving the resulting system of four simultaneous equations for $\mathcal{R}$, and using $T_G = 1 - |\mathcal{R}|^2$, we finally obtain the transmittance as

$$\begin{aligned}T_G = \cos^2\phi\cos^2\theta[\cos^2(q_x D)\cos^2\phi\cos^2\theta \\ + \sin^2(q_x D)(1 + \sin\phi\sin\theta)^2]^{-1}.\end{aligned} \tag{9}$$

For normal incidence, the transmission probability is $T_G = 1$ and it is independent of the barrier height V_0 and width D, like that in the linear case. The transmission probability becomes unity also when $q_x D = \pi n,\ n \in \mathbb{Z}$. The linear case is obtained by setting $\alpha = 0$ in Eqs. (2) and (6), and repeating the above-mentioned calculations. It can also be obtained as a limiting process (see Sec. B of Ref. [46]) and we recover

$$q_x^2 = \frac{(E_G - V_0)^2}{\hbar^2 v_F^2} - k^2\sin^2\phi, \tag{10}$$

the same result as Ref. [19].

In Fig. 2 (top) we show a polar plot of the transmission coefficient T and T_G to compare the predictions of the linear versus the generalized Dirac structures. We considered the parameters of graphene reported in Ref. [29], $a = 1.4$ Å, $t = 3$ eV, and $t' = -0.3$ eV. Moreover, the barrier is $V_0 = 285$ meV high and $D = 96$ nm wide. As demonstrated above,

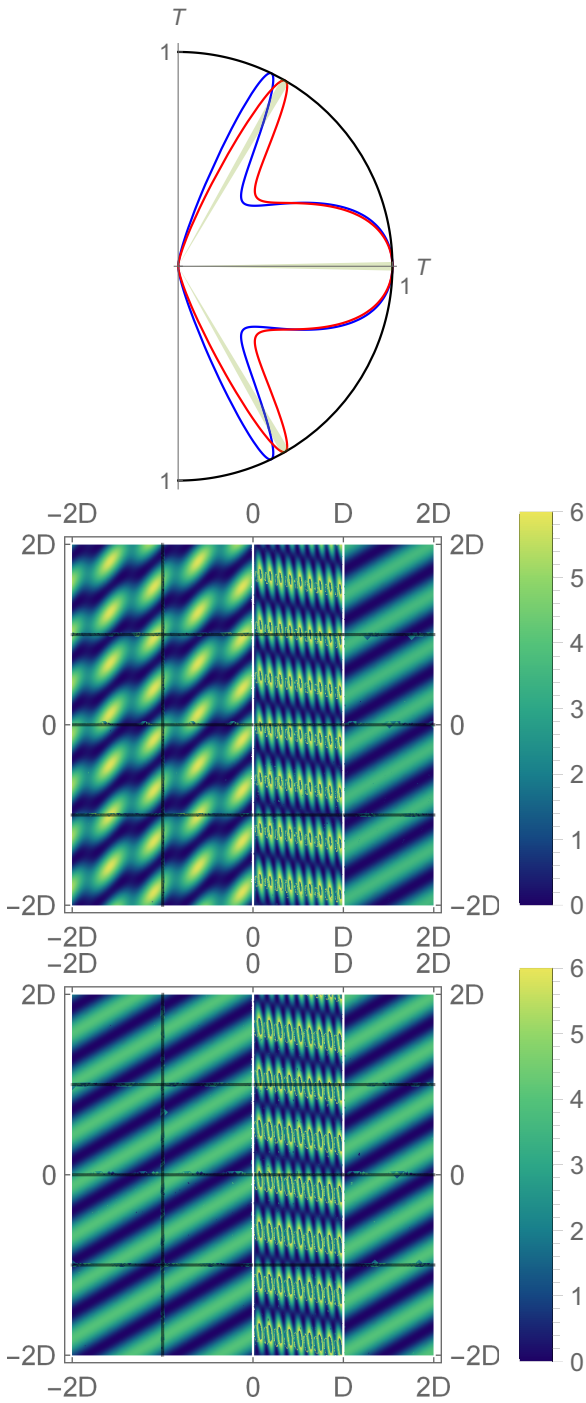

FIG. 2. Top: Transmission probability T and T_G through a $V_0 = 285$-meV-high and $D = 96$-nm-wide barrier as a function of the incidence angle ϕ, both with $k = k_0 = 1.3407 \times 10^8$ m^{-1}. The blue curve is the linear prediction of T and the red curve the prediction T_G with the GDS. The black curve corresponds to unit transmission. Center: Probability density in the x-y plane of the superposition of two plane waves, $\Phi = \Psi(k_0, 0) + \Psi(k_0, \pi/3)$, considering only the linear regime. Bottom: Probability density $||\Phi||^2$ using the generalized Dirac structure. In all plots, the barrier is placed parallel to the armchair direction and the horizontal (vertical) axis is the x (y) coordinate.

the angle at which transmission is maximized depends on the momentum of the incoming wave. Therefore, we specifically selected the momentum $k = k_0 = 1.3407 \times 10^8$ m^{-1} for which the barrier becomes transparent ($T_G = 1$) at $\phi = 0, \pm\pi/3$, where trigonal warping is null. For k_0 the energy in the linear regime is $E = 84.4638$ meV while considering the GDS is $E_G = 84.226$ meV. The barrier is placed parallel to the armchair direction. The blue curve is the linear prediction of T as in Ref. [19] and the red curve the prediction T_G with the generalized Dirac structure (9). The green-shadowed areas are regions for the incident angle ϕ where trigonal warping can be neglected. In these areas, Eq. (6) represents correctly Klein tunneling up to $O((ka)^2)$. The transmission in the GDS is shifted compared to the linear case because Klein tunneling is susceptible to changes in the energy of incoming quasiparticles which results from the different dispersion relation. In general the transmission coefficient is different for the two cases for the same angle of incidence ϕ for a given wave number k.

Since Eq. (6) is a linear differential equation, then it is also a correct representation in the subspace spanned by the plane waves with incident angle $\phi \in (-\delta, \delta) \cup (\pi/3 - \delta, \pi/3 + \delta) \cup (-\pi/3 - \delta, -\pi/3 + \delta)$.

In Fig. 2 (center and bottom), we show the interference pattern produced by the superposition of two incoming waves at different angles of incidence, $\Phi = \Psi(k_0, 0) + \Psi(k_0, \pi/3)$, considering the linear regime and the GDS, respectively. For the GDS and the chosen angles of incidence (0 and $\pi/3$), the transmittance is $T_G = 1$ and, thus, both incoming waves are fully transmitted. As a consequence, the wave function after the barrier (region C) is the same as in region A. On the contrary, in the linear case $T \neq 1$ for the angle $\pi/3$. Thus, a certain fraction of the incoming wave is reflected back, creating an interference pattern in region A.

As demonstrated previously, it is possible to simulate the effect of minimum length on Klein tunneling in graphene by showing that the transmittance $T_G(E, \phi)$, for some specific angles, is sensitive to the discrete topology ($T_G \neq T$). Probing this effect experimentally would be challenging because it requires a careful positioning of the potential barrier with respect to the lattice and because it requires resolving the transmission coefficient in angle and energy. However, this may be possible with actual experimental techniques. Indeed, time-resolved photoemission electron microscopy (TR-PEEM) is capable of resolving the dynamics of charge carriers in time, space, energy, and momentum with nanometer and femtosecond resolutions [51]. In addition, laser beams can generate well-controlled photoinduced currents in graphene [52]. Therefore, we propose to use a pump-probe experiment where a mid-infrared pump photoexcites charge carriers and makes them scatter on the potential barrier. Because this happens on short time scales (approximately the wave period of $\Delta t \sim 200$ fs), charge carriers travel large enough distances to go through the potential barrier ($\sim$200 nm $\gtrsim D$), but low enough to reduce possible scatterings with impurities and defects (ballistic regime). The laser field intensity required to accelerate charge carriers to the required energy is estimated as $I \sim 10^5$ W/cm^2, using $\Delta p \sim eE_\ell \Delta t$ where E_ℓ is the laser field strength. This is below the intensity of known mid-infrared laser sources [53].

Furthermore, it is also possible to scan many scattering angles by modifying the laser polarization. The resulting dynamics can then be analyzed with the PEEM as a function of the pump-probe time delay. Using the scattering dynamics of the distribution of charge carriers measured from the PEEM, we expect to be able to evaluate the transmission coefficient.

In this Letter, we have studied the effect of next-to-nearest atom hopping on quantum transport in graphene. This was analytically done by analyzing the tight-binding model beyond the linear regime. The effective quantum dynamics obtained from such an approximation was used to obtain an emergent generalized Dirac structure, which captured the effects of discrete topology and which is reminiscent of Lorentz-breaking quantum gravity models. This technique is general and could be applied to any Dirac materials with an underlying discrete topology. It was proposed that such effects can be tested by measuring transmittance through *n*-*p*-*n* graphene junctions using a pump-probe experiment.

Here we point out that the analogy with quantum gravity can be clearly seen by considering its analogy with doubly special relativity (DSR) [36]. In DSR, the Planck energy acts as the maximal possible energy, and the smooth manifold structure of spacetime breaks beyond that energy. Furthermore, due to DSR, the behavior of spacetime also changes at intermediate energies, and this can be observed in effects like the breaking of Lorentz symmetry. In graphene, the situation is similar, as we have a maximum energy scale at which the interatomic bounds break, along with any smooth structure. This again has similar implications for intermediate-energy phenomena in graphene. Therefore, graphene can also be used as an analog for Lorentz-violating phenomena, which remain very elusive in high-energy particle physics experiments (see Refs. [54,55]).

To conclude, it would be interesting to generalize this work by incorporating the effects of a trigonal warping term. This could be done by certain asymmetric expansion of the generalized momentum in terms of the standard low-energy momentum. This will naturally furnish us a nonisotropic GUP reflecting the nonisotropy of space itself [56]. It will be useful to use this formalism for the study of Klein tunneling and other phenomena in graphene with a trigonal warping term.

A.C.A. acknowledges the support of Consejo Nacional de Ciencia y Tecnología (CONACyT-México) under Grant No. FORDECYT-PRONACES/61533/2020. F.F.G. and S.M. would like to thank Pierre Lévesque for discussions on the experimental proposal.

[1] G. W. Semenoff, Condensed-Matter Simulation of a Three-Dimensional Anomaly, Phys. Rev. Lett. **53**, 2449 (1984).
[2] K. S. Novoselov, A. K. Geim, S. V. Morozov, D. Jiang, M. I. Katsnelson, I. V. Grigorieva, S. V. Dubonos, and A. A. Firsov, Two-dimensional gas of massless Dirac fermions in graphene, Nature (London) **438**, 197 (2005).
[3] A. H. Castro Neto, F. Guinea, N. M. R. Peres, K. S. Novoselov, and A. K. Geim, The electronic properties of graphene, Rev. Mod. Phys. **81**, 109 (2009).
[4] M. I. Katsnelson and K. S. Novoselov, Graphene: New bridge between condensed matter physics and quantum electrodynamics, Solid State Commun. **143**, 3 (2007).
[5] D. Allor, T. D. Cohen, and D. A. McGady, Schwinger mechanism and graphene, Phys. Rev. D **78**, 096009 (2008).
[6] B. Dóra and R. Moessner, Nonlinear electric transport in graphene: Quantum quench dynamics and the Schwinger mechanism, Phys. Rev. B **81**, 165431 (2010).
[7] F. Fillion-Gourdeau and S. MacLean, Time-dependent pair creation and the Schwinger mechanism in graphene, Phys. Rev. B **92**, 035401 (2015).
[8] A. Golub, R. Egger, C. Müller, and S. Villalba-Chávez, Dimensionality-Driven Photoproduction of Massive Dirac Pairs near Threshold in Gapped Graphene Monolayers, Phys. Rev. Lett. **124**, 110403 (2020).
[9] V. M. Pereira, V. N. Kotov, and A. H. Castro Neto, Supercritical Coulomb impurities in gapped graphene, Phys. Rev. B **78**, 085101 (2008).
[10] Y. Wang, D. Wong, A. V. Shytov, V. W. Brar, S. Choi, Q. Wu, H.-Z. Tsai, W. Regan, A. Zettl, R. K. Kawakami, S. G. Louie, L. S. Levitov, and M. F. Crommie, Observing atomic collapse resonances in artificial nuclei on graphene, Science **340**, 734 (2013).
[11] F. Fillion-Gourdeau, P. Levesque, and S. MacLean, Plunging in the Dirac sea using graphene quantum dots, Phys. Rev. Res. **2**, 033472 (2020).
[12] N. Stander, B. Huard, and D. Goldhaber-Gordon, Evidence for Klein Tunneling in Graphene *p*-*n* Junctions, Phys. Rev. Lett. **102**, 026807 (2009).
[13] A. F. Young and P. Kim, Quantum interference and Klein tunnelling in graphene heterojunctions, Nat. Phys. **5**, 222 (2009).
[14] E. Sonin, Effect of Klein tunneling on conductance and shot noise in ballistic graphene, Phys. Rev. B **79**, 195438 (2009).
[15] M. Sanderson, Y. S. Ang, and C. Zhang, Klein tunneling and cone transport in AA-stacked bilayer graphene, Phys. Rev. B **88**, 245404 (2013).
[16] M. T. Greenaway, E. E. Vdovin, A. Mishchenko, O. Makarovsky, A. Patanè, J. Wallbank, Y. Cao, A. Kretinin, M. Zhu, S. Morozov, *et al.*, Resonant tunnelling between the chiral Landau states of twisted graphene lattices, Nat. Phys. **11**, 1057 (2015).
[17] T. Low, S. Hong, J. Appenzeller, S. Datta, and M. S. Lundstrom, Conductance asymmetry of graphene *p*-*n* junction, IEEE Trans. Electron Devices **56**, 1292 (2009).
[18] D. Perconte, F. A. Cuellar, C. Moreau-Luchaire, M. Piquemal-Banci, R. Galceran, P. R. Kidambi, M.-B. Martin, S. Hofmann, R. Bernard, B. Dlubak, *et al.*, Tunable Klein-like tunnelling of high-temperature superconducting pairs into graphene, Nat. Phys. **14**, 25 (2018).
[19] M. I. Katsnelson, K. S. Novoselov, and A. K. Geim, Chiral tunnelling and the Klein paradox in graphene, Nat. Phys. **2**, 620 (2006).
[20] P. E. Allain and J. N. Fuchs, Klein tunneling in graphene: Optics with massless electrons, Eur. Phys. J. B **83**, 301 (2011).

[21] C. W. J. Beenakker, Colloquium: Andreev reflection and Klein tunneling in graphene, Rev. Mod. Phys. **80**, 1337 (2008).
[22] Y. Avishai and Y. B. Band, Chiral tunneling in single-layer graphene with Rashba spin-orbit coupling: Spin currents, Phys. Rev. B **103**, 134445 (2021).
[23] Y. Avishai and Y. B. Band, Klein bound states in single-layer graphene, Phys. Rev. B **102**, 085435 (2020).
[24] A. F. M. Rodrigues da Silva, M. S. M. Barros, A. J. Nascimento, A. L. R. Barbosa, and J. G. G. S. Ramos, Klein paradox in chaotic Dirac billiards, Ann. Phys. **405**, 256 (2019).
[25] L. Z. Szabó, M. G. Benedict, A. Czirják, and P. Földi, Relativistic electron transport through an oscillating barrier: Wave-packet generation and Fano-type resonances, Phys. Rev. B **88**, 075438 (2013).
[26] E. Prada, P. San-Jose, and L. Brey, Zero Landau Level in Folded Graphene Nanoribbons, Phys. Rev. Lett. **105**, 106802 (2010).
[27] A. Contreras-Astorga, F. Correa, and V. Jakubský, Super-Klein tunneling of Dirac fermions through electrostatic gratings in graphene, Phys. Rev. B **102**, 115429 (2020).
[28] S. Lee, V. Stanev, X. Zhang, D. Stasak, J. Flowers, J. S. Higgins, S. Dai, T. Blum, X. Pan, V. M. Yakovenko, *et al.*, Perfect Andreev reflection due to the Klein paradox in a topological superconducting state, Nature (London) **570**, 344 (2019).
[29] A. Kretinin, G. L. Yu, R. Jalil, Y. Cao, F. Withers, A. Mishchenko, M. I. Katsnelson, K. S. Novoselov, A. K. Geim, and F. Guinea, Quantum capacitance measurements of electron-hole asymmetry and next-nearest-neighbor hopping in graphene, Phys. Rev. B **88**, 165427 (2013).
[30] S.-H. Zhang and W. Yang, Perfect transmission at oblique incidence by trigonal warping in graphene P-N junctions, Phys. Rev. B **97**, 035420 (2018).
[31] J. M. Pereira, F. M. Peeters, A. Chaves, and G. A. Farias, Klein tunneling in single and multiple barriers in graphene, Semicond. Sci. Technol. **25**, 033002 (2010).
[32] R. Logemann, K. J. A. Reijnders, T. Tudorovskiy, M. I. Katsnelson, and S. Yuan, Modeling Klein tunneling and caustics of electron waves in graphene, Phys. Rev. B **91**, 045420 (2015).
[33] J. M. Pereira, Jr., F. M. Peeters, R. N. Costa Filho, and G. A. Farias, Valley polarization due to trigonal warping on tunneling electrons in graphene, J. Phys.: Condens. Matter **21**, 045301 (2009).
[34] O. Bahat-Treidel, O. Peleg, M. Grobman, N. Shapira, M. Segev, and T. Pereg-Barnea, Klein Tunneling in Deformed Honeycomb Lattices, Phys. Rev. Lett. **104**, 063901 (2010).
[35] A. Iorio, P. Pais, I. A. Elmashad, A. F. Ali, M. Faizal, and L. I. Abou-Salem, Generalized Dirac structure beyond the linear regime in graphene, Int. J. Mod. Phys. D **27**, 1850080 (2018).
[36] G. Amelino-Camelia, Quantum-spacetime phenomenology, Living Rev. Relativ. **16**, 5 (2013).
[37] S. Hossenfelder, Minimal length scale scenarios for quantum gravity, Living Rev. Relativ. **16**, 2 (2013).
[38] S. Das and E. C. Vagenas, Universality of Quantum Gravity Corrections, Phys. Rev. Lett. **101**, 221301 (2008).
[39] A. F. Ali, S. Das, and E. C. Vagenas, Proposal for testing quantum gravity in the lab, Phys. Rev. D **84**, 044013 (2011).
[40] M. O. Goerbig, Electronic properties of graphene in a strong magnetic field, Rev. Mod. Phys. **83**, 1193 (2011).
[41] P. Plochocka, C. Faugeras, M. Orlita, M. L. Sadowski, G. Martinez, M. Potemski, M. O. Goerbig, J. N. Fuchs, C. Berger, and W. A. de Heer, High-Energy Limit of Massless Dirac Fermions in Multilayer Graphene using Magneto-Optical Transmission Spectroscopy, Phys. Rev. Lett. **100**, 087401 (2008).
[42] G. Amelino-Camelia, J. Ellis, N. E. Mavromatos, and D. V. Nanopoulos, Distance measurement and wave dispersion in a Liouville-string approach to quantum gravity, Int. J. Mod. Phys. A **12**, 607 (1997).
[43] G. Amelino-Camelia, Phenomenology of Planck-scale Lorentz-symmetry test theories, New J. Phys. **6**, 188 (2004).
[44] R. Aloisio, P. Blasi, P. L. Ghia, and A. F. Grillo, Probing the structure of space-time with cosmic rays, Phys. Rev. D **62**, 053010 (2000).
[45] S. Das, E. C. Vagenas, and A. F. Ali, Discreteness of space from GUP II: Relativistic wave equations, Phys. Lett. B **690**, 407 (2010).
[46] See Supplemental Material at http://link.aps.org/supplemental/10.1103/PhysRevB.105.L161401 for more detailed calculations.
[47] A. F. Ali, S. Das, and E. C. Vagenas, Discreteness of space from the generalized uncertainty principle, Phys. Lett. B **678**, 497 (2009).
[48] H. Falomir, J. Gamboa, M. Loewe, and M. Nieto, Graphene and non-Abelian quantization, J. Phys. A: Math. Theor. **45**, 135308 (2012).
[49] H. Falomir, M. Loewe, E. Muñoz, and A. Raya, Optical conductivity and transparency in an effective model for graphene, Phys. Rev. B **98**, 195430 (2018).
[50] H. Falomir, E. Muñoz, M. Loewe, and R. Zamora, Optical conductivity in an effective model for graphene: Finite temperature corrections, J. Phys. A: Math. Theor. **53**, 015401 (2020).
[51] C. Tusche, A. Krasyuk, and J. Kirschner, Spin resolved bandstructure imaging with a high resolution momentum microscope, Ultramicroscopy **159**, 520 (2015), special issue: LEEM-PEEM 9.
[52] T. Higuchi, C. Heide, K. Ullmann, H. B. Weber, and P. Hommelhoff, Light-field-driven currents in graphene, Nature (London) **550**, 224 (2017).
[53] H. A. Hafez, X. Chai, A. Ibrahim, S. Mondal, D. Férachou, X. Ropagnol, and T. Ozaki, Intense terahertz radiation and their applications, J. Opt. **18**, 093004 (2016).
[54] A. G. Cohen and S. L. Glashow, Very Special Relativity, Phys. Rev. Lett. **97**, 021601 (2006).
[55] N. A. Shah and M. A. H. Ahsan, Quantization of non-Abelian gauge theory in graphene, Int. J. Geom. Methods Mod. Phys. **18**, 2150048 (2021).
[56] R. B. Mann, I. Husin, H. Patel, M. Faizal, A. Sulaksono, and A. Suroso, Testing short distance anisotropy in space, Sci. Rep. **11**, 7474 (2021).